Applied Catalysis A: General 501 (2015) 10–16

Contents lists available at ScienceDirect

Applied Catalysis A: General

journal homepage: www.elsevier.com/locate/apcata

Ammoxidation of propane to acrylonitrile over silica-supported Fe-Bi nanocatalysts

Richard D. Adams[a,*], Gaya Elpitiya[a], Konstantin Khivantsev[b], Douglas Blom[c], Oleg S. Alexeev[b,**], Michael D. Amiridis[b,***]

[a] Department of Chemistry and Biochemistry, University of South Carolina, Columbia, SC 29208, USA
[b] Department of Chemical Engineering, University of South Carolina, Columbia, SC 29208, USA
[c] Electron Microscopy Center, University of South Carolina, Columbia, SC 29208, USA

ARTICLE INFO

Article history:
Received 30 January 2015
Received in revised form 16 April 2015
Accepted 18 April 2015
Available online 24 April 2015

Keywords:
Propane ammoxidation
Mixed FeBi oxides
Nanoparticles
Cluster-derived catalyst
XPS
HRSTEM
EDS

ABSTRACT

Ammoxidation of propane to acrylonitrile was examined over a Fe_3BiO_x/SiO_2 sample prepared by thermal decarbonylation of $[Et_4N][Fe_3(CO)_{10}(\mu_3\text{-Bi})]$ on the surface of mesoporous silica. Catalytic measurements performed at 500 °C showed that this sample yields 49% acrylonitrile selectivity at 36% propane conversion when a 5.5%C_3H_8/30%O_2/11%NH_3/He balance reaction mixture was used at a GHSV of 1360 h^{-1}. HRSTEM, EDS, and XPS measurements indicate that mixed Fe_3BiO_6 oxide particles less than 2 nm in size were formed on the surface of this material under reaction conditions. A Fe/Bi atomic ratio in these particles is approximately 3:1 and the Fe and Bi ions both are in the +3 oxidation state. A Fe-Bi/SiO_2 sample prepared by co-impregnation of individual Fe and Bi salts had very low activity and low selectivity for acrylonitrile formation from propane under similar experimental conditions due to larger sizes of particles formed under reaction conditions and enrichment of their surface with Fe.

1. Introduction

The ammoxidation of propene to acrylonitrile (Eq. (1)) catalyzed by bismuth molybdates is one of world's largest commercial processes for the production of a commodity chemical [1–3].

$$C_3H_6 + 3/2O_2 + NH_3 \rightarrow CH_2CHCN + 3H_2O \quad (1)$$

Experimental and computational results have indicated that the critical alkene activation step occurs at the methyl group of propene by a Bi-O function in the bismuth-molybdate catalysts [4–9]. Supported catalysts incorporating bismuth have also been shown to catalyze the oxidation of different aromatic and alkane compounds [10–12]. There is considerable interest in developing selective oxidation and ammoxidation reactions by using less expensive and widely available saturated hydrocarbons and considerable efforts have been made to utilize propane as a feedstock for the synthesis of acrylonitrile [13–33].

Literature reports have shown that iron-antimony oxide catalysts exhibit significant activity for the oxidation and ammoxidation of propane [34] and propene [35]. Zhuang and Catlow [36] have examined possible mechanisms of propane ammoxidation over $FeSbO_4$ catalysts by computational methods and identified two possible pathways: one that starts with hydrogen abstraction from the methylene group in propane and proceeds through a propylene intermediate and a second one that starts with hydrogen abstraction from one of the methyl groups. These two mechanisms have similar energy barriers, resulting in similar temperatures at which the products are formed. Moreover, the antimony and oxygen atoms were found to play key roles in the CH activation steps of the hydrocarbon.

While antimony and bismuth have similar chemical properties, there are virtually no literature examples of propane ammoxidation over iron-bismuth catalytic materials. A number of years ago, it was reported that ternary iron-bismuth-phosphorus oxide systems are effective catalysts for the ammoxidation of propene [37] and acrolein [38]. More recently, it has been shown that catalytic properties of supported bimetallic catalysts incorporating bismuth can be significantly improved by using bismuth-transition metal carbonyl cluster complexes as precursors [39,40]. Accordingly, we have now examined the ability of SiO_2-supported iron-bismuth nanoparticles prepared from iron-bismuth carbonyl cluster

* Corresponding author. Tel.: +1 8037776781.
** Corresponding author. Tel.: +1 8037779914.
*** Corresponding author. Tel.: +1 3124133350.
E-mail addresses: adamsrd@mailbox.sc.edu (R.D. Adams), alexeev@cec.sc.edu (O.S. Alexeev), amiridis@uic.edu (M.D. Amiridis).

http://dx.doi.org/10.1016/j.apcata.2015.04.025
0926-860X/

complexes to catalyze the reaction of propane ammoxidation to form acrylonitrile. These results are reported herein.

2. Experimental

Reagent grade solvents were dried by the standard procedures and freshly distilled under nitrogen prior to use. $[Et_4N][Fe_3(CO)_{10}(\mu_3\text{-Bi})]$, **1** was prepared as reported elsewhere [41]. The $Fe(CO)_5$ (STREM) and $NaBiO_3$ (Sigma–Aldrich) compounds were used in the preparation routine without further purification.

2.1. Catalyst preparation

The cluster-derived catalyst (further denoted as Fe_3BiO_x/SiO_2) was prepared from the bimetallic precursor **1**: 520 mg of **1** was dissolved in 100 mL of CH_2Cl_2. 5.00 g of Davisil 923 (pore size 30 Å, 100–200 mesh, Grace Davison) mesoporous silica support was added to this solution and the slurry was stirred under nitrogen for 24 h. The solvent was then slowly removed under vacuum. Finally, the impregnated sample was heated under vacuum to 200 °C for a period of approximately 2 h to remove the CO ligands, yielding 5.25 g of supported catalyst with 5% metal loading.

For comparison, the Fe-Bi/SiO_2 sample with a Fe/Bi molar ratio of 3 was prepared by co-impregnation: 85.9 mg of $FeBr_2$ and 41.9 mg of $BiCl_3$ were dissolved in 100 mL of acetonitrile (NCMe). Following the addition of 1.00 g of Davisil 923 mesoporous silica support, the mixture was stirred under nitrogen for 24 h. After the solvent was slowly removed by evacuation, the resulting material was heated under vacuum to 200 °C for a period of approximately 2 h to yield 1.05 g of catalyst with 5% metal loading.

2.2. Characterizations

2.2.1. High resolution scanning transmission electron microscopy

High resolution scanning transmission electron microscopy (HRSTEM) was performed at the University of South Carolina Electron Microscopy Center using a JEOL 2100F 200 kV FEG-STEM/TEM equipped with a CEOS C_s corrector on the illumination system. The geometrical aberrations were measured and controlled to provide less than a $\pi/4$ phase shift of the incoming electron wave over the probe-defining aperture of 17.5 mrad. High angle annular dark-field (HAADF) high resolution scanning transmission electron microscopy images were acquired on a Fischione Model 3000 HAADF detector with a camera length such that the inner cut-off angle of the detector was 50 mrad. The scanning acquisition was synchronized to the 60 Hz AC electrical power to minimize 60 Hz noise in the images and a pixel dwell time of 15.8 μs was used. Particle size distributions were obtained by observing and including at least 300 particles from several different images. The surface-averaged size of particles was calculated as $\sum_i n_i d_i^3 / \sum_i n_i d_i^2$ (where n_i is the number of particles with the d_i diameter).

2.2.2. X-ray photoelectron spectroscopy (XPS)

A Kratos AXIS Ultra DLD X-ray photoelectron spectrometer equipped with a monochromatic Al-Kα source operated at 1.5 keV and 150 W was used for XPS measurements. The pass energy was fixed at 40 eV for the detailed scans. A charge neutralizer was used to compensate for the surface charging during the photoemission. The Si 2p signal with a binding energy of 103.3 eV was used as an internal reference for calibration of the O 1s, Fe 2p, and Bi 4f binding energy values. All binding energies reported in this work were measured with a precision of ±0.2 eV. XPS data were analyzed by nonlinear curve fitting using the PeakFit 4.12 software. In all cases, a linear-type background was subtracted from the spectra and a curve fit was performed using the minimum number of Voigt G/L-type peaks that provides a good fit. In each case, the fitting routine was completed when the coefficient of determination (R^2) value was 0.98 or higher.

2.2.3. Catalytic measurements

The catalytic tests were performed in a Pyrex single-pass fixed-bed reactor at atmospheric pressure and temperatures in the 350–500 °C range. The temperature inside the reactor was monitored by a thermocouple extended into the catalyst bed. Samples in powder form (0.3 g) were diluted with quartz (2 g), loaded into the reactor, and heated to 300 °C under He for a period of approximately 5 h prior to measurements. Two reaction feeds (i.e., 5.5%C_3H_8/30%O_2/11%NH_3/He and 8%C_3H_8/20%O_2/9%NH_3/He) with O_2/C_3H_8 ratios of 5.5 and 2.5, respectively, were used to determine how catalytic properties of SiO_2-supported Fe-Bi samples in propane ammoxidation depend on the O_2 content. In each case, the total volumetric flow rate of the reactant mixture was held at 2.7 and 9 mL/min (1 atm, 25 °C), yielding a corresponding Gas Hourly Space Velocity (GHSV) of 408 and 1360 h^{-1}, respectively. The feed and the reaction products were analyzed with an on-line gas chromatograph (HP 5890, Agilent) equipped with TCD and FID detectors and carboxen-1000 and plot-Q columns. A carboxen-1000 column was used for the analysis of CO_2, while a plot-Q column (30 m, 0.53 mm ID, Supelco) was used for the analysis of hydrocarbons. All the lines leading to the gas chromatograph were heated at 220 °C using heating tapes in order to avoid condensation and polymerization of the acrylonitrile. In the absence of a catalyst, there was no measurable conversion of C_3H_8. The results reported herein were obtained after steady-state conditions were reached at each temperature. In order to do so, measurements were carried out for at least 4 h at each temperature with 30 min intervals between the reactor effluent analysis injections. No deactivation of the catalysts was observed even after 2 days of testing at the same temperature and reproducible results were obtained at different temperatures regardless of the heating/cooling protocol used, indicating the absence of thermal deactivation either.

Propane conversion was determined as the molar amount of propane consumed over the total molar amount of propane used in the feed. Product selectivities were determined as the molar amount of each product formed divided by the molar amount of propane consumed and adjusted for differences in carbon stoichiometry (i.e., multiplied by the ratio of carbon atoms in the specific product over the number of carbon atoms in propane). Product yields were determined as the product of propane conversion multiplied by product selectivities.

3. Results and discussion

Results of the catalytic measurements obtained at the GHSV of 1360 h^{-1} for the cluster-derived Fe_3BiO_x/SiO_2 catalyst are shown in Fig. 1, where the propane conversion and the selectivities for the various products formed are plotted as a function of reaction temperature. The limited catalytic activity observed at temperatures below 450 °C (i.e., propane conversions below 10%) is associated primarily with the oxidation of propane, as indicated by the formation of CO_2 as the main reaction product. The formation of acrylonitrile (AcCN), acetonitrile (ACN), propene, and ethene was first detected at 420 °C. Consistent with previous literature reports [29–34,36], the appearance of propene among other reaction products suggests that it may be an intermediate for the propane ammoxidation reaction. Both the selectivity to different products and the propane conversion continue to increase with reaction temperature. For example, the propane conversion was as high

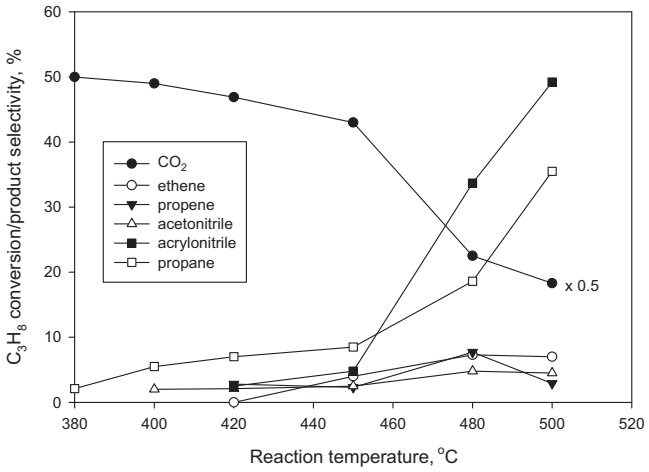

Fig. 1. Propane conversion and product selectivities for the ammoxidation of propane over a cluster-derived Fe_3BiO_x/SiO_2 catalyst as a function of reaction temperature (feed composition: 5.5%C_3H_8/30%O_2/11%NH_3/He balance; GHSV = 1360 h^{-1}).

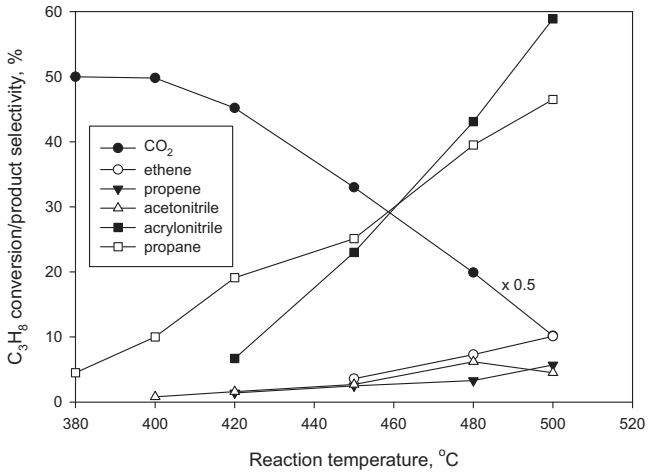

Fig. 2. Propane conversion and product selectivities for the ammoxidation of propane over a cluster-derived Fe_3BiO_x/SiO_2 catalyst as a function of reaction temperature (feed composition: 8%C_3H_8/20%O_2/9%NH_3/He balance; GHSV = 408 h^{-1}).

as 36% at 500 °C and the selectivity to AcCN reached 49%, while the yield was 18%. Corresponding changes for other reaction products were evidently less prominent as ACN, propene, and ethene selectivities remained below 10% in the 420–500 °C temperature range.

When lower space velocities and, therefore, longer contact times were used in experiments with Fe_3BiO_x/SiO_2, higher propane conversions were observed at the same temperature, while the selectivity to AcCN remained similar, resulting in higher yields, as shown in Table 1. For example, the AcCN yield increased from 7 to 19% and from 18 to 29% at reaction temperatures of 480 and 500 °C, respectively, when the GHSV was decreased from 1360 to 408 h^{-1}. A similar trend was also observed for ACN, since the ACN selectivity was not significantly affected in this case either.

A comparison was also attempted between the cluster-derived Fe_3BiO_x/SiO_2 sample and a Fe-Bi/SiO_2 catalyst of the same composition prepared by co-impregnation. The results collected for Fe-Bi/SiO_2 at 500 °C and GHSV of 1360 h^{-1} (Table 1) indicate a much lower propane conversion and no measurable production of either AcCN or ACN, although the formation of propene was observed (2.4% yield) in addition to CO_2.

The effect of the feed composition on the production of AcCN over Fe_3BiO_x/SiO_2 was examined next. For example, at 500 °C and GHSV of 408 h^{-1}, a decrease in the O_2/C_3H_8 ratio from 5.5 to 2.5 resulted in a moderate decrease of propane conversion from 59 to 47%. At the same time, the AcCN selectivity increased from 48 to 59%, while the AcCN yield (28%) remained unchanged. The complete results collected at these conditions are shown in Fig. 2.

Typical HAADF HRSTEM images collected for a cluster-derived Fe_3BiO_x/SiO_2 sample that was used for propane ammoxidation at 500 °C are shown in Fig. 3. Highly dispersed particles less than 2 nm in size constitute the majority of particles present on these images. The particle size distribution obtained for this sample is relatively narrow with approximately 96% of the particles being in the size range of 0.5–2.0 nm. Several particles with sizes in the 2.5–4.5 nm range can be also found in HRSTEM images. While the fraction of these larger particles is relatively small and does not exceed 4%, their contribution to an average particle size is significant, as the surface-averaged size of the particles calculated from these data was found to be of approximately 2 nm (Fig. 4). Energy dispersive X-ray spectroscopy (EDS) measurements performed on random particles of different sizes shows the presence of both Fe and Bi in these particles with atomic concentrations of approximately 75 and 25%, respectively, yielding approximately a 3:1 Fe/Bi atomic ratio, which is consistent with the Fe/Bi ratio found in the cluster precursor complex.

In addition, to determine the elemental distribution of Bi and Fe on the surface of Fe_3BiO_x/SiO_2, spatially resolved EDS measurements were carried out on a relatively wide sample area (around 0.08 μm^2). Fig. 5A and B shows the relevant EDS chemical maps of the Bi Lα and Fe Kα characteristic X-rays, respectively, acquired at a pixel size of 10 nm. These images are unfiltered, representing the

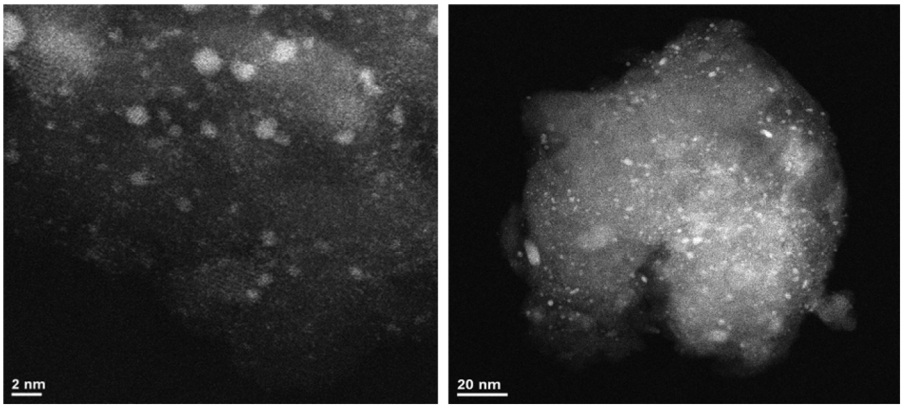

Fig. 3. HAADF HRSTEM images of a cluster-derived Fe_3BiO_x/SiO_2 catalyst that was used for propane ammoxidation at 500 °C.

Table 1
Summary of the effects of space velocity and temperature on propane conversion and product distribution over the cluster-derived Fe_3BiO_x/SiO_2 catalyst.

Sample/reaction conditions	Propane conversion, %	AcCN selectivity, %	ACN selectivity, %	C_3H_6 selectivity, %	AcCN yield, %
Fe_3BiO_x/SiO_2, GHSV = 1360 h^{-1}, T = 480 °C	19	34	5	8	7
Fe_3BiO_x/SiO_2, GHSV = 408 h^{-1}, T = 480 °C	51	36	5	3	19
Fe_3BiO_x/SiO_2, GHSV = 1360 h^{-1}, T = 500 °C	36	49	5	3	18
Fe_3BiO_x/SiO_2, GHSV = 408 h^{-1}, T = 500 °C	59	48	4	4	29
Fe-Bi/SiO_2, GHSV = 1360 h^{-1}, T = 500 °C	12	<1	<1	20	<1

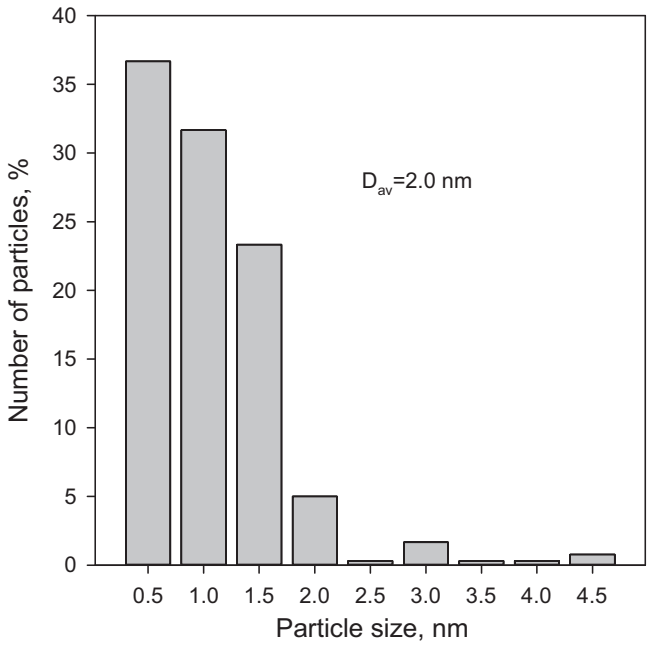

Fig. 4. Particle size distribution characterizing a cluster-derived Fe_3BiO_x/SiO_2 catalyst that was used for propane ammoxidation at 500 °C.

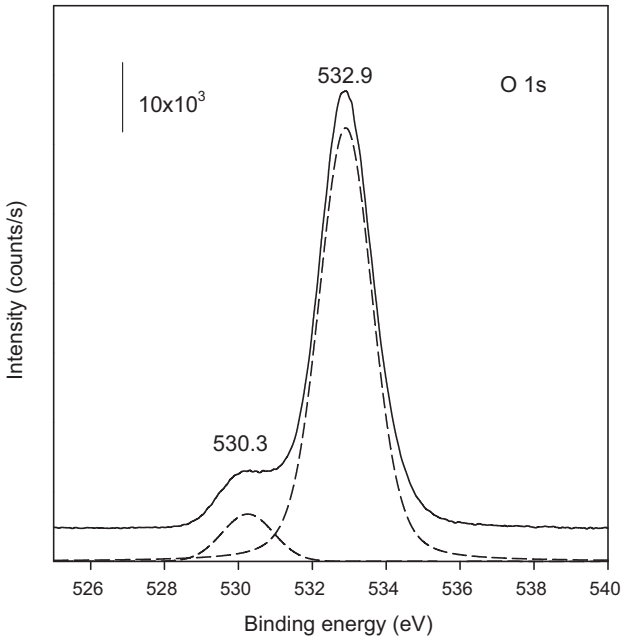

Fig. 6. O 1s region of the XPS spectrum of a cluster-derived Fe_3BiO_x/SiO_2 catalyst used for propane ammoxidation at 500 °C (solid line) and deconvolution results (dotted line).

raw intensities of the characteristic Bi and Fe edges at each point in the map. A comparison of these maps shows that the bright areas enriched in Fe in Fig. 5B closely correspond to the areas enriched in Bi in Fig. 5A. This further suggests that Fe and Bi are closely associated on the surface of this catalytic material.

To clarify the nature of particles formed in the spent Fe_3BiO_x/SiO_2 sample, the surface of this material was examined by X-ray photoelectron spectroscopy (XPS) and the spectra collected for the O 1s, Fe 2p, and Bi 4f regions are shown in Figs. 6–8. The O 1s spectrum includes two components with binding energies of 532.9 and 530.3 eV (Fig. 6). Consistent with previous literature reports [42], a relatively strong O 1s peak at 532.9 eV originates from Si-O contributions of the SiO_2 support. In agreement with such an assignment, the O/Si atomic ratio for this peak was found to be of approximately 2.0. A weaker O 1s contribution at 530.3 eV clearly represents the species formed on the SiO_2 surface. The specific assignment for this peak is less certain since differences in O 1s binding energies reported previously for various Fe oxides (i.e., 529.9–530.9 eV) [43], Bi_2O_3 (529.4 eV) [44], and $FeBiO_3$ (529.5 eV) [45] species are small and, therefore, O 1s peaks originating from Fe-O, Bi-O, and Fe-O-Bi are expected to overlap if any combinations of such species are formed on the support surface. Regardless of this uncertainty, the presence of this peak in the XPS spectrum indicates that the particles observed on the surface of the spent Fe_3BiO_x/SiO_2 material by HRSTEM are oxides in nature.

The Bi 4f region can be fitted with a pair of peaks with FWHM values of 1.7 eV, a spin-orbit split of 5.3 eV, and binding energies of 159.3 and 164.6 eV which correspond to Bi $4f_{7/2}$ and $4f_{5/2}$ core

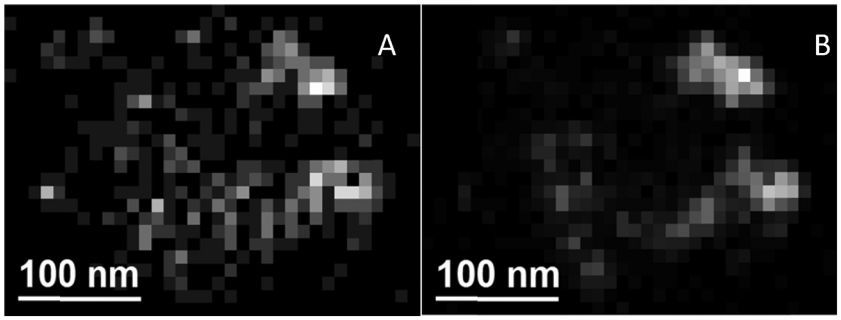

Fig. 5. EDS maps of the Bi Lα (A) and Fe Kα (B) characteristic X-rays acquired at a pixel size of 10 nm for a cluster-derived Fe_3BiO_x/SiO_2 catalyst that was used for propane ammoxidation at 500 °C.

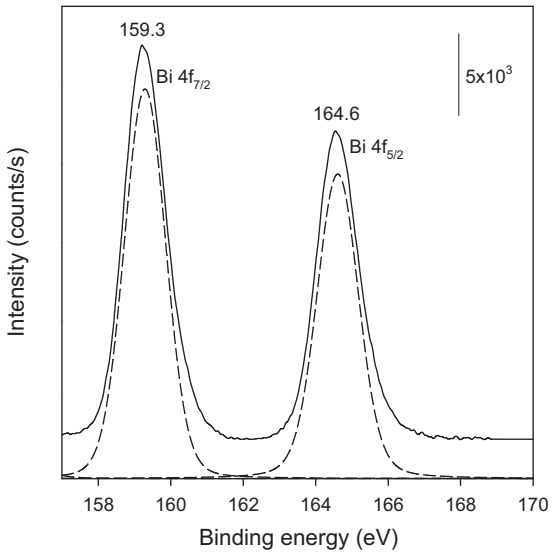

Fig. 7. Bi 4f region of the XPS spectrum of a cluster-derived Fe_3BiO_x/SiO_2 catalyst used for propane ammoxidation at 500 °C (solid line) and deconvolution results (dotted line).

level emissions, respectively (Fig. 7). These binding energies are slightly higher than those reported previously for Bi_2O_3 (i.e., 158.8 and 164.2 eV) [46] but match closely with the Bi $4f_{7/2}$ and $4f_{5/2}$ binding energies reported for various mixed oxides, including $FeBiO_3$ (i.e., 159.1 and 164.4 eV, respectively) [47]. While higher binding energies of Bi in the latter case can be explained by electron transfer from the Bi cations towards other components of mixed oxides [46], the Bi $4f_{7/2}$ and $4f_{5/2}$ binding energies determined from our spectra are consistent with Bi^{3+} cations being present on the surface of the spent Fe_3BiO_x/SiO_2 material, as no any contributions from Bi^{5+} cations (expected at 161.5 and 167.0 eV for $4f_{7/2}$ and $4f_{5/2}$ core level emissions, respectively) can be observed in XPS spectra.

The Fe 2p XPS region is more complex and includes besides $2p_{3/2}$ and $2p_{1/2}$ spin-orbit doublet components the corresponding satellite peaks at 718.2 and 731.7 eV, respectively (Fig. 8). Moreover, minimum two components are required to include in the fit for each Fe $2p_{3/2}$ and Fe $2p_{1/2}$ emission line in order to achieve a R^2

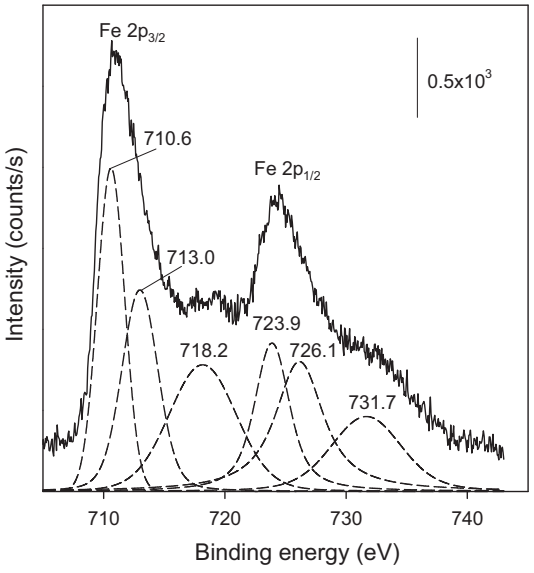

Fig. 8. Fe 2p region of the XPS spectrum of a cluster-derived Fe_3BiO_x/SiO_2 catalyst used for propane ammoxidation at 500 °C (solid line) and deconvolution results (dotted line).

value of 0.98 or higher. As a result, two types of Fe ions can be identified in the spectrum with Fe $2p_{3/2}$ and $2p_{1/2}$ binding energies of 710.6/713.0 eV and 723.9/726.1 eV, respectively, and a spin-orbit split of approximately 13.2 eV. These binding energies are fully consistent with those reported in the literature [43,45,46] for Fe^{3+} ions in FeO(OH), Fe_3O_4, Fe_2O_3, and $FeBiO_3$ compounds. Since the presence of satellite peaks is typical for Fe $2p_{3/2}$ and $2p_{1/2}$ emission lines of Fe^{3+} ions and contributions from Fe^{2+} ions (expected at 709.5 eV) cannot be found in the spectrum, we can conclude with confidence that only Fe^{3+} ions are present on the surface of the spent Fe_3BiO_x/SiO_2 material. These Fe^{3+} ions are obviously not identical since both the Fe $2p_{3/2}$ and $2p_{1/2}$ core level emission lines split into two components.

Since XPS provides average information from the surface, several assignments are possible. For example, one could suggest that the Fe $2p_{3/2}$ and $2p_{1/2}$ peaks with binding energies of 710.6 and 723.9 eV, respectively, represent Fe-O-Bi species, while the second set of Fe $2p_{3/2}$ and $2p_{1/2}$ peaks with binding energies of 713.0 and 726.1 eV, respectively, originates from Fe^{3+} cations not interacting with Bi. In other words, such an assignment suggests that not all oxide particles formed on the surface of SiO_2 incorporate both the Fe and Bi ions but at least some of them incorporate only Fe ions.

Alternatively, one can suggest that all particles formed on the SiO_2 surface consist of mixed FeBi oxides but Fe^{3+} ions in these particles have two different coordination environments. This suggestion is similar to what have been reported previously for several pure Fe oxides and $FeBiO_3$ nanoparticles. For example, Fe^{3+} ions in octahedral and tetrahedral coordination with characteristic Fe $2p_{3/2}$ binding energies in the 710.2–712.3 eV and 712.9–713.7 eV range, respectively, were found to be present in Fe_3O_4 and Fe_2O_3 [43]. Likewise, it has been reported that the Fe $2p_{3/2}$ region of $FeBiO_3$ nanoparticles splits into two components with binding energies of 710.3 and 712.1 eV, consistent with the presence of Fe-O-Bi links in which Fe^{3+} ions have two different coordination environments [45].

In attempts to narrow the assignment choices for the Fe 2p region and to determine the composition of particles formed on the SiO_2 surface more precisely, XPS spectra in O 1s, Fe 2p, and Bi 4f regions were quantified using peak areas and atomic sensitivity factors that were included in the Kratos software by the manufacture. The results obtained indicate that particles formed on the surface of the spent Fe_3BiO_x/SiO_2 sample consist of 61.6% O, 27.7% Fe, and 10.7% Bi, yielding a Fe/Bi atomic ratio of 2.6 and a net composition of surface species of approximately $Fe_{2.6}BiO_{5.8}$. The Fe/Bi atomic ratio determined from XPS is fairly close to a Fe/Bi atomic ratio of 3 estimated from EDS measurements, suggesting that the Fe/Bi ratio remains nearly unchanged when the cluster precursor is transformed into a mixed FeBi oxide on the surface of silica under reaction conditions. Taking into account that the Fe and Bi ions both are in the 3+ oxidation state, the net composition of the surface species thus formed can be further approximated as Fe_3BiO_6 to balance the overall charge. However, since $FeBiO_3$ is the most common composition representing mixed FeBi oxides [45,46], one could also suggest that Fe_3BiO_6 species can be represented by a 1:1 ratio of $FeBiO_3$ and Fe_2O_3. While such a suggestion clearly assumes the existence of two types of Fe^{3+} ions due to the presence of Fe-O-Bi and O-Fe-O on the support surface and is consistent with fitting results for the Fe 2p region, it is also assumes that the atomic ratio between Fe species of Fe_2O_3 and those of $FeBiO_3$ must be 2:1. In contrast to this expectation, our results show a 1:1 ratio between Fe^{3+} species with characteristic Fe $2p_{3/2}$ binding energies of 713.0 and 710.6 eV, strongly suggesting that this is not the case. Therefore, it is more likely that particles observed on the surface of SiO_2 in the spent Fe_3BiO_x/SiO_2 material consist of a pure Fe_3BiO_6 mixed oxide in which Fe^{3+} ions have two distinct coordination environments. Our attempts to clarify further the structure

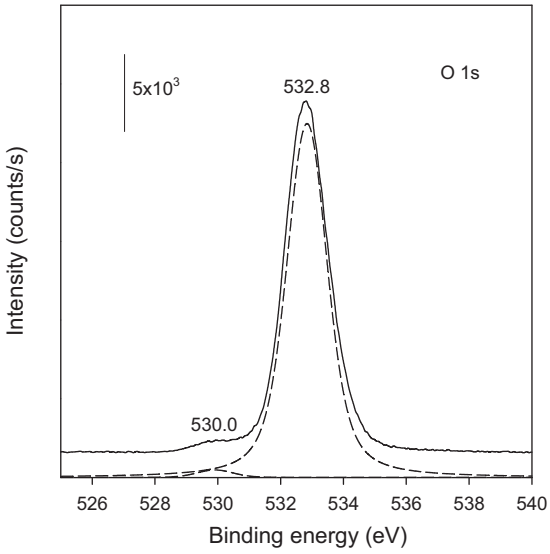

Fig. 9. O 1s region of the XPS spectrum of a co-impregnated Fe-Bi/SiO_2 catalyst used for propane ammoxidation at 500 °C (solid line) and deconvolution results (dotted line).

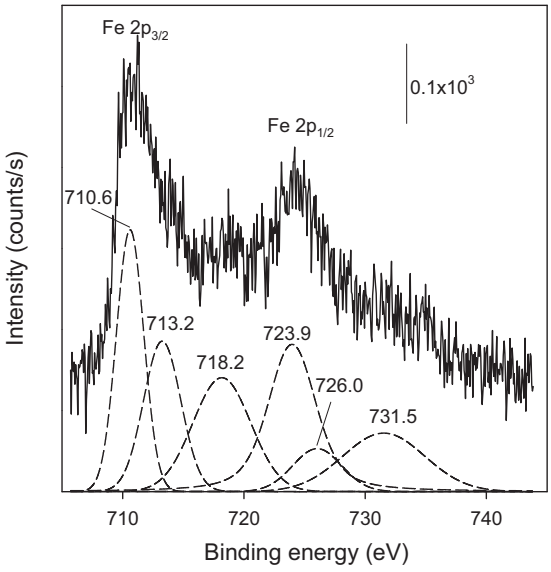

Fig. 11. Fe 2p region of the XPS spectrum of a co-impregnated Fe-Bi/SiO_2 catalyst used for propane ammoxidation at 500 °C (solid line) and deconvolution results (dotted line).

of these particles by XRD were not successful due to their small sizes.

For comparison purposes, XPS measurements were also performed over the spent Fe-Bi/SiO_2 material prepared by co-impregnation. The spectra collected for the O 1s, Fe 2p, and Bi 4f regions are shown in Figs. 9–11. The O 1s spectrum includes two components with binding energies of 532.8 and 530.0 eV (Fig. 9). The former peak clearly represents the support oxygen, as the O/Si atomic ratio of 2.1 for this peak is consistent with the SiO_2 stoichiometry. As we discussed above, the O 1s peak at 530.0 eV most likely represents Fe-O, Bi-O, and Fe-O-Bi contributions of the oxide species formed on the SiO_2 surface. Similar to the case of the cluster-derived sample, the Bi 4f region includes a pair of peaks with binding energies of 159.2 and 164.5 eV assigned to Bi $4f_{7/2}$ and $4f_{5/2}$ core level emissions, respectively (Fig. 10). Furthermore, two types of Fe ions can also be identified in the Fe 2p spectrum of this sample with Fe $2p_{3/2}$ and $2p_{1/2}$ binding energies of 710.6/713.2 eV and 723.9/726.0 eV, respectively, together with the corresponding satellite peaks at 718.2 and 731.5 eV, respectively (Fig. 11).

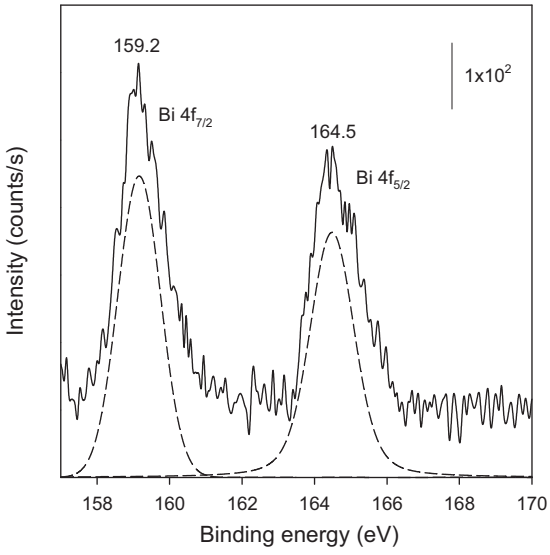

Fig. 10. Bi 4f region of the XPS spectrum of a co-impregnated Fe-Bi/SiO_2 catalyst used for propane ammoxidation at 500 °C (solid line) and deconvolution results (dotted line).

A comparison of these data with those included in Figs. 6–8 further shows that the co-impregnated sample has the set of peaks in the Bi 4f and Fe 2p regions with binding energies closely matching the corresponding binding energies of the cluster-derived sample. This result suggests that surface species of similar nature are formed in both cases and these species incorporate iron and bismuth, both of which are in +3 oxidation state.

However, some substantial differences between co-impregnated and cluster-derived samples were also observed. For example, Table 2 shows a comparison of the O/Si, Fe/Si, and Bi/Si atomic intensity ratios for these two materials. It has been shown previously that atomic intensity ratios of different peaks in XPS spectra are directly related to the dispersion of metal oxide species formed [48,49]. The larger the ratio, the more dispersed the oxide phase [48,49]. As can be noted from data of Table 2, the O/Si, Fe/Si, and Bi/Si atomic intensity ratios characterizing the cluster-derived Fe_3BiO_x/SiO_2 sample are significantly larger than those calculated for the co-impregnated Fe-Bi/SiO_2 sample, strongly suggesting that the surface species formed in the former case are better dispersed.

It is further evident that the Fe/Bi ratio characterizing the co-impregnated Fe-Bi/SiO_2 sample is approximately 6, which is higher than the Fe/Bi ratio of 2.7 estimated for the cluster-derived sample. This result clearly indicates that the 3:1 Fe/Bi ratio initially intended for surface species in the co-impregnated material does not hold and in fact, the surface species formed are enriched with iron. Therefore, we can infer that the dispersion of surface species formed and the Fe/Bi ratio in these species are two important factors that govern ammoxidation activity of this type materials, considering that a bifunctional-type of mechanism is involved in the ammoxidation of the propane [3].

Table 2.
XPS atomic intensity ratios of samples used for propane ammoxidation.

Sample	O/Si	Fe/Si	Bi/Si
Fe_3BiO_x/SiO_2	0.17	0.08	0.03
Fe-Bi/SiO_2	0.01	0.03	0.005

4.. Conclusions

Our results have shown that the cluster-derived Fe_3BiO_x/SiO_2 material prepared from the $[Et_4N][Fe_3(CO)_{10}(\mu_3\text{-Bi})]$ precursor is an effective catalyst for the ammoxidation of propane at temperatures above 500 °C. Nearly uniform particles with an average size of approximately 2 nm are formed on the surface of this material under reaction conditions. EDS and XPS measurements indicate that these particles incorporate both the Fe and Bi components with a 3:1 Fe/Bi atomic ratio and both of these elements are in the +3 oxidation state in the active material. The cluster-derived Fe_3BiO_x/SiO_2 sample performs moderately better than FeSb oxide catalysts used for propane ammoxidation [29–33], but it is not as effective as the MoV(Nb,Ta)(Te,Sb)O combinations also used for the same reaction [3,26]. The presence of propene in the effluent suggests that propene may be an intermediate in the catalytic process, as has been also recognized by others [29–34,36].

Acknowledgments

This research was supported by the National Science Foundation CHE-1111496 (RDA).

References

[1] R.K. Grasselli, in: G. Ertl, H. Knozinger, J. Weitkamp (Eds.), Handbook of Heterogeneous Catalysis, 5, VCH, Publishers, Weinheim, 1997, pp. 2302–2326.
[2] J.F. Brazdil, in: A. Seidel (Ed.), Kirk-Othmer Encyclopedia of Chemical Technology, Wiley-Interscience, New York, 1991, pp. 397–414.
[3] R.K. Grasselli, C.G. Lugmair, A.F. Volpe Jr., Top. Catal. 54 (2011) 595–604.
[4] T.A. Hanna, Coord. Chem. Rev. 248 (2004) 429–440.
[5] W.A. Goddard III, K. Chenoweth, S. Pudar, A.C.T. van Duin, M.-J. Cheng, Top. Catal. 50 (2008) 2–18.
[6] Y.H. Jang, W.A. Goddard III, J. Phys. Chem. B 106 (2002) 5997–6013.
[7] A. Getsoian, V. Shapovlov, A.T. Bell, J. Phys. Chem. C 117 (2013) 7123–7137.
[8] A.K. Rappé, Mol. Phys. 102 (2004) 289–299.
[9] S. Pudar, J. Oxgaard, K. Chenoweth, A.C.T. van Duin, W.A. Goddard III, J. Phys. Chem. C 111 (2007) 16405–16415.
[10] D. Dumitriu, R. Bârjega, L. Frunza, D. Macovei, T. Hu, Y. Xie, V.I. Pârvulescu, S. Kaliaguine, J. Catal. 219 (2003) 337–351.
[11] J. Zhao, G. Qian, F. Li, J. Zhu, S. Ji, L. Li, Chin. J. Catal. 33 (2012) 771–776.
[12] G. Qian, D. Ji, G. Lu, R. Zhao, Y. Qi, J. Suo, J. Catal. 232 (2005) 378–385.
[13] R.K. Grasselli, Top. Catal. 21 (2002) 79–88.
[14] R.K. Grasselli, Catal. Today 99 (2005) 23–31.
[15] Y. Ishii, S. Sakaguchi, T. Iwahama, Adv. Synth. Catal. 343 (2001) 393–427.
[16] T.T. Punniyamurthy, S. Velusamy, J. Iqbal, Chem. Rev. 105 (2005) 2329–2363.
[17] M.A. Soria, P. Ruiz, E.M. Gaigneaux, Catal. Today 203 (2013) 40–47.
[18] C. O'Neill, E.E. Wolf, Catal. Today 156 (2010) 124–131.
[19] M.M. Bettahar, G. Costentin, L. Savary, J.C. Lavalley, Appl. Catal. A 145 (1996) 1–48.
[20] R.K. Grasselli, C.G. Lugmair, A.F. Volpe, A. Andersson, J.D. Burrington, Catal. Today 157 (2010) 33–38.
[21] M. Vaarkamp, U. Takashi, Appl. Catal. A 174 (1998) 99–107.
[22] A. Kaddouri, C. Mazzocchia, E. Tempesti, Appl. Catal. A 180 (1999) 271–275.
[23] H.W. Zanthoff, S. Schaefer, G.U. Wolf, Appl. Catal. A 164 (1997) 105–117.
[24] P. Biswas, J. Woo, V.V. Guliants, Catal. Commun. 12 (2010) 58–63.
[25] I. Ramli, P. Botella, F. Ivars, W.P. Meng, S.M.M. Zawawi, H.A. Ahangar, S. Hernandez, J.M.L. Nieto, J. Mol. Catal. A 342–343 (2011) 50–57.
[26] R.K. Grasselli, J.D. Burington, D.J. Buttrey, P. DeSanto Jr., C.G. Lugmair, A.F. Volpe Jr., T. Weingand, Top. Catal. 23 (2003) 5–22.
[27] R.K. Grasselli, A.F. Volpe Jr., Top. Catal. 57 (2014) 1124–1137.
[28] J. Yu, Y. Xu, V.V. Guliants, Top. Catal. 57 (2014) 1145–1151.
[29] R. Catani, G. Centi, F. Trifiro, R.K. Grasselli, Ind. Eng. Chem. Res. 31 (1992) 107–119.
[30] M.O. Guerrero-Perez, M.A. Pena, J.L.G. Fierro, M.A. Banares, Ind. Eng. Chem. Res. 45 (2006) 4537–4543.
[31] H.-W. Zanthoff, S.A. Bucholz, Catal. Lett. 49 (1997) 213–217.
[32] S. Albonetti, G. Blanchard, P. Buratin, T.J. Cassidy, S. Masetti, F. Trifiro, Catal. Lett. 45 (1997) 119–123.
[33] G. Centi, F. Marchi, Stud. Surf. Sci. Catal. 101 (1996) 277–286.
[34] M. Bowker, C.R. Bicknell, P. Kerwin, Appl. Catal. A 136 (1996) 205–229.
[35] M.D. Allen, G.J. Hutching, M. Bowker, Appl. Catal. A 217 (2001) 33–39.
[36] C. Zhuang, C.R.A. Catlow, J. Phys. Chem. C 112 (2008) 9783–9797.
[37] K. Miyake, H. Oka, H. Sakamoto, Y. Harano, T. Imoto, J. Chem. Soc. Jpn. 2 (1972) 284–289.
[38] H. Oka, K. Miyake, Y. Harano, T. Imoto, J. Appl. Chem. Biotechnol. 25 (1975) 663–670.
[39] R.D. Adams, M. Chen, G. Elpitiya, M.E. Potter, R. Raja, ACS Catal. 3 (2013) 3106–3110.
[40] R. Raja, R.D. Adams, D.A. Blom, W.C. Pearl Jr., E. Gianotti, J.M. Thomas, Langmuir 25 (2009) 7200–7204.
[41] K.H. Whitmire, C.B. Lagrone, M.R. Churchill, J.C. Fettinger, L.V. Biondi, Inorg. Chem. 23 (1984) 4227–4232.
[42] P. Yang, L. Liu, J. Mo, W. Yang, Semicond. Sci. Technol. 25 (2010) 045017/1–045017/45017.
[43] S. Poulin, R. França, L. Moreau-Bélanger, E. Sacher, J. Phys. Chem. C 114 (2010) 10711–10718.
[44] D. Barreca, F. Morazzoni, G.A. Rizzi, R. Scotti, E. Tondello, Phys. Chem. Chem. Phys. 3 (2001) 1743–1749.
[45] T. Gao, Z. Chen, Y. Zhu, F. Niu, Q. Huang, L. Qin, X. Sun, Y. Huang, Mater. Res. Bull. 59 (2014) 6–12.
[46] Y. Schuhl, H. Baussart, R. Delobel, M. Le Bras, J.-M. Leroy, J. Chem. Soc. Faraday Trans. 79 (1983) 2055–2069.
[47] K. Jiang, J.J. Zhu, J.G. Wu, J. Sun, Z.G. Hu, J.H. Chu, ACS Appl. Mater. Interfaces 3 (2011) 4844–4852.
[48] Y. Okamoto, T. Imanaka, S. Teranishi, J. Phys. Chem. 85 (1981) 3798–3805.
[49] B.M. Reddy, B. Chowdhury, P.G. Smirniotis, Appl. Catal. A 211 (2001) 19–30.